Model-free parameter tuning with continuous genetic algorithm: application to virtual controlled object-based active vibration controller

Heisei Yonezawa[1†], Ansei Yonezawa[2] and Itsuro Kajiwara[3]

[1]Division of Mechanical and Aerospace Engineering, Hokkaido University, Sapporo, Japan
(Tel : +81-80-4039-9406; E-mail: yonezawah@eng.hokudai.ac.jp)
[2]Department of Mechanical Engineering, Kyushu University, Fukuoka, Japan
(Tel : +81-90-2893-3160; E-mail: ayonezawa@mech.kyushu-u.ac.jp)
[3]Division of Mechanical and Aerospace Engineering, Hokkaido University, Sapporo, Japan
(Tel : +81-11-706-6390; E-mail: ikajiwara@eng.hokudai.ac.jp)

Abstract

Active vibration control is a powerful approach to provide higher damping effects over a broad range of frequencies. However, most of them generally involve a modeling process of a controlled structure, complicating the controller design. The main contribution of this study is to present a novel tuning scheme of a model-free active oscillation controller based on continuous genetic algorithm (CGA), which can simplify a controller design process by eliminating the need for plant modeling. The model-free controller is developed using a virtual controlled object (VCO) as its foundation. VCO makes it possible to construct an active damping controller without knowing any specifications of a real controlled structure. In the offline tuning of the design variables of the controller, we use a reference-controlled object (RCO) - a single-degree-of-freedom (SDOF) structure defined by the designer - to assess the damping level instead of the actual controlled structure model. This evaluation is feasible due to the robustness of the VCO-based design, which accommodates variations in the controlled object structures. The application of the CGA, which has the global search ability, enables automatically specifying the optimal parameter values without costly trial-and-error works. The effectiveness of the auto-optimized model-free damping controller is demonstrated through numerical examples across different mechanical systems, with comparisons made to a trial-and-error-tuned controller. The main finding is that the controller can reduce the vibration amplitudes even though plant modeling of the actual controlled objects is not accompanied at all. As the representative results, the resonance peaks of two different cantilever plates were suppressed by 14.38 dB and 27.13 dB in the low-frequency band. The detailed-specification-independent nature provided by the model-free design makes it possible to apply the resultant controller to various structures because the robustness is enforced.

Keywords: Active oscillation damping, Model-free control, Virtual controlled object, Continuous genetic algorithm, Optimization

1. INTRODUCTION

Vibration control is demanded to enhance precisions of mechanical systems.[1,2,3] For challenging vibration problems such as a vehicle suspension system,[4] powertrain vibrations,[5,6] and a ball-screw drive system,[7] various vibration suppression approaches have been presented. Among them, due to the good damping effects, active oscillation reduction is widely used.[8,9,10] Nevertheless, the necessary plant modeling is expensive and time-consuming. Model-free control that is building of control systems without requiring a detailed plant model can lower development costs and workloads.

Without relying on specific models of real controlled systems, numerous researchers have explored developing different control systems. Approaches to creating model-free control systems include methods based on fuzzy logic,[11] neural networks (NN),[12] active disturbance rejection control (ADRC),[13,14] and data-driven techniques.[15] For example, one study constructed an ADRC-based active vibration controller for seismically excited building structures.[16] A fuzzy NN algorithm was also applied to realize an active tuned mass damper.[17] To manage an active suspension system, a feed-forward deep neural network (DNN) controller was introduced,[18] incorporating a network training procedure utilizing the backpropagation algorithm. The effectiveness of employing adaptive intelligent control algorithms for active vibration control has been reviewed in detail.[19]

However, despite their notable outcomes on superior control performance, the conventional model-free approaches have several difficulties which degrade the practicability such as sensitiveness to changes in characteristics of plants, complicated design processes requiring many tasks for a designer, and lack of a systematic design policy. Moreover, a controller optimization task (i.e., parameter tuning) is rarely spotlighted despite its importance even though many efforts have been dedicated to creating model-free active control systems.[20,21,22] Some works discussed an optimization technique for control parameters,[23,24]; however, most of previous studies require a mathematical model of a controlled object in the tuning process.

Compared to existing model-free control approaches, model-free active oscillation control based on a virtual controlled object (VCO) is easier to implement and has a simpler controller design process.[25,26] In this method, only a single-degree-of-freedom (SDOF) system, namely VCO, and an actuator model are used for designing an oscillation controller. Based on the quantitative design condition established in the previous literature,[25] the suitable VCO to realize model-free control can be specified. Once the VCO is designed, the controller can be systematically developed using established control theories such as LQR. However, a problem exists in that the VCO-based design approach involves some tuning parameters, indicating the need for a practical and simple parameter tuning scheme.

Drawing from examples of optimization algorithms in practice,[6,27] we propose a novel method for tuning parameters in VCO-based model-free controllers. Unlike previous approaches that rely on gradient-based optimization methods,[28,29] our approach utilizes a continuous genetic algorithm (CGA)[30,31,32] because of its global search capabilities. Initially, we derive the model-free vibration control system by integrating the SDOF VCO between an actuator model and the actual structure being controlled. Next, the controller's parameters are tuned by CGA. In the tuning algorithm, the damping efficiency of the controller is assessed using a reference-controlled object (RCO), a structure specified by the designer, rather than actual plant models. The VCO controller's robustness enables this replacement. As an evaluation index of the controller's performance, a loss function is introduced. Offline iterative simulations are conducted using the RCO, and the design parameters of the controller are optimized to minimize the loss function through CGA. This study uses this tuning scheme for a VCO-based linear quadratic regulator (LQR)[28] and investigates its damping performance by simulation analysis with unknown mechanical oscillation systems. The main contributions and technical novelties of this research are outlined as follows:

1. Compared to conventional model-based active damping systems, the novel contribution of this work is to present a CGA-based model-free auto-design strategy for an active oscillation controller, which does not involve any plant modeling of a real controlled system during all controller design procedures. In the optimization process for control parameters, necessity of a real plant model can be eliminated by replacing it with VCO and RCO appropriately established. This design scheme can decrease the controller development costs. In this paper, the proposed strategy is applied to tuning the VCO-based LQR.
2. The new integration of CGA and the RCO-based controller tuning allows for obtaining a more globally optimized solution with simple implementation, in contrast to prior studies.[28,29]
3. The proposed controller design method is validated via numerical examples with several different mechanical structures involving severe characteristic changes. Assessing the proposed technique against a trial-and-error approach highlights its excellent attenuation and robustness.

The rest of this paper is structured as follows. Section 2 outlines the design of a model-free controller utilizing the VCO concept. Section 3 introduces the proposed approach, which is the RCO-CGA-based parameter tuning method. Section 4 applies the tuning scheme to VCO-based LQR. Section 5 conducts comparative simulation tests. Section 6 provides the conclusion of the paper.

2. VCO-BASED MODEL-FREE DESIGN

In the proposed control system, the employment of an electromagnetic proof-mass actuator indicated in Fig. 1 is assumed. According to its driving principle, this actuator is modeled as an SDOF configuration.[25]

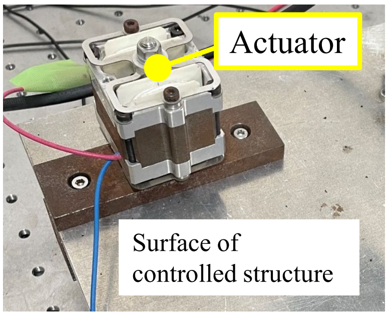

Fig. 1 Electromagnetic proof-mass actuator.

Figure 2(a) depicts the mechanical system in active damping. The actuator's mass, stiffness, and damping are denoted, respectively, by m_0, k_0, and c_0. The displacement of the actuator and the specific point on the actual controlled object where vibration reduction is targeted are represented by x_0 and x_1, respectively. The purpose of the active vibration controller is to manage the actuator with a control input u in order to diminish the vibration x_1 at the designated damping point.

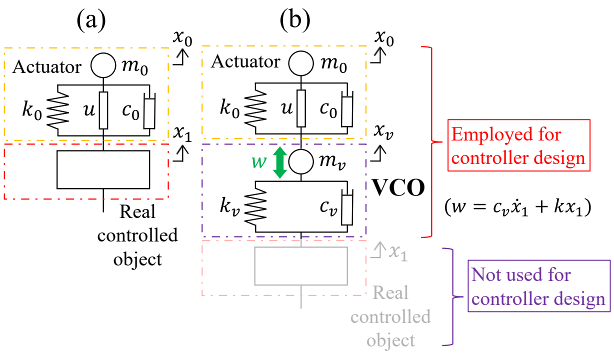

Fig. 2 Active damping setup: (a) the real mechanical system and (b) the system used for designing the model-free controller.

Table 1 Parameters for active controller design.

Symbols	Values	Unit
m_v	1.0×10^{-5}	kg
k_v	7.0×10^{5}	N/m
c_v	0.0	Ns/m
c_0	1.186	Ns/m
k_0	3518	N/m
m_0	0.2013	kg

The proposed controller design relies on the VCO-based model-free control in order to eliminate the need for plant modeling of actual controlled structures. The basic idea is detailed in our previous literature.[25] The diagram in Fig. 2(b) illustrates the system used for designing a model-free controller, incorporating a VCO to facilitate this design process between the actuator and the actual controlled object. In this setup, the displacement of the VCO is indicated as x_v, with its mass, stiffness, and damping parameters represented as m_v, k_v, and c_v, which are essential variables in the design. The fundamental concept of our model-free design technique is that x_1 is indirectly attenuated by controlling x_v, with the proper design of VCO being viewed as the dummy controlled object.[25,26,28] This replacement with the properly designed VCO eliminates the need for usage of the real plant model because only the VCO and actuator's specifications are necessary for developing an active damping controller that aims to achieve indirect control of x_1. In simpler terms, the 2DOF system, comprising only the actuator and VCO, is used for the control design, leading to a model-free approach.

The parameters m_v and k_v should be determined for realizing model-free control. It is specifically needed to set $x_v \approx x_1$ in the controlled frequency band (CFB) in order to realize the indirect active damping of x_1 via x_v. To analyze the condition to realize model-free design, the following transfer function H_{xvx1} from x_1 to x_v is considered.[25]

$$H_{xvx1}(s) = \frac{\hat{x}_v(s)}{\hat{x}_1(s)} = \frac{Num(s)}{Den(s)} \tag{1}$$

$$Num(s) = (m_0 s^2 + k_0 + c_0 s)(c_v s + k_v) \tag{2}$$

$$Den(s) = (m_0 s^2 + c_0 s + k_0)\{m_v s^2 + (k_0 + k_v) + (c_0 + c_v)s\} - (c_0 s + k_0)^2 \tag{3}$$

where the Laplace transformation of x_v and x_1 are represented as $\hat{x}_v(s)$ and $\hat{x}_v(s)$, respectively, with Laplace operator s.

The required condition $x_v \approx x_1$, which allows for indirect active damping for x_1 via x_v, is translated into satisfying $H_{xvx1}(s) \approx 1$ in a desired CFB. Therefore, $H_{xvx1}(s) \approx 1$ is regarded as promising one of the design policies for specifying appropriate VCO parameters, i.e., m_v and k_v. According to Eqs. (2) and (3), a combination of a sufficiently great value of k_v and a minute value of m_v results in $H_{xvx1}(s) \approx 1$. A more quantitative and clearer guideline to specify VCO has been founded in the form of the following inequality.[25]

$$\left\{\left(\frac{(\Omega_k^{cont})^2}{k_0} - \frac{1}{m_0}\right)k_v + (\Omega_k^{cont})^2\right\}\frac{1}{m_v} > \left(\frac{(\Omega_k^{cont})^2}{k_0} - \frac{1}{m_0}\right)(\Omega_k^{cont})^2, \qquad (k = 1, 2) \tag{4}$$

where Ω_1^{cont} and Ω_2^{cont} ($\Omega_2^{cont} > \Omega_1^{cont} \geq \sqrt{k_0/m_0}$) denote the lower and upper frequency limits of the controlled band, respectively. Previous research has demonstrated that $x_v \approx x_1$ within the controlled frequency band can be achieved by meeting the design criteria for m_v and k_v.[25] It is important to note that the specifications of the actual controlled structure, such as models or parameters, do not influence Eqs. (1)-(4) aside from the CFB. Consequently, a suitable VCO can be designed without needing detailed information about the actual controlled structure. The values for the actuator and VCO specifications used in this paper are listed in Table 1.

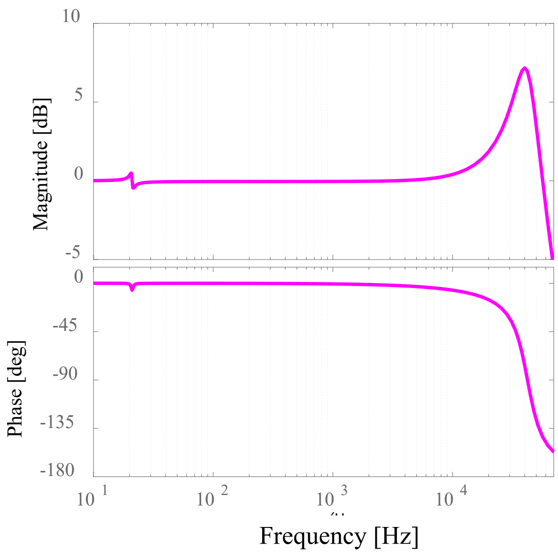

Fig. 3 Bode diagram of the transfer property from a response of the real structure to that of VCO.

Figure 3 illustrates the Bode plot of $H_{xvx1}(jw)$, where $|H_{xvx1}(jw)| \approx 1$ is maintained within the CFB, defined as $f \in (\Omega_1^{cont} = 5.0 \times 10^1$ Hz, $\Omega_2^{cont} = 3.0 \times 10^3$ Hz). Within the CFB, there is little phase lag.

For the system depicted in Fig. 2(b), the following state equation is derived[25,26]:

$$x_{mf} = [x_v \quad x_0 \quad \dot{x}_v \quad \dot{x}_0]^T \tag{5}$$

$$\dot{x}_{mf} = A_{mf}x_{mf} + B_{mf1}w + B_{mf2}u \tag{6}$$

$$A_{mf} = \begin{bmatrix} 0 & 0 & 1 & 0 \\ 0 & 0 & 0 & 1 \\ -\frac{k_0 + k_v}{m_v} & \frac{k_0}{m_v} & -\frac{c_0 + c_v}{m_v} & \frac{c_0}{m_v} \\ \frac{k_0}{m_0} & -\frac{k_0}{m_0} & \frac{c_0}{m_0} & -\frac{c_0}{m_0} \end{bmatrix} \tag{7}$$

$$B_{mf1} = \begin{bmatrix} 0 & 0 & \frac{1}{m_v} & 0 \end{bmatrix}^T \tag{8}$$

$$B_{mf2} = \begin{bmatrix} 0 & 0 & -\frac{1}{m_v} & \frac{1}{m_0} \end{bmatrix}^T \tag{9}$$

$$w = c_v\dot{x}_1 + k_v x_1. \tag{10}$$

Equation (6) does not incorporate details about the specific object being controlled, making the controller design for Eq. (6) independent of the model. By ensuring that $x_v \approx x_1$, the controller designed using established model-based control theories indirectly damps x_1 of the actual plant. In the real-world feedback control, the measured output x_1, which is nearly equal to x_v, is used for performing the closed-loop control.

It should be noted that the VCO-based model-free controller design has the following limitations and assumptions.

1. As discussed in Eq. (4), it is necessary to know the frequency range in which the natural frequencies of the controlled structure may vary.
2. The actuator needs to be a proof-mass-type actuator, as shown in Figs. 1 and 2, and should be modeled as a single-degree-of-freedom (SDOF) system.
3. The controlled structures must have sufficient space for actuator installation, and collocation of the sensor and actuator is required.

3. TUNING METHOD BASED ON RCO AND CGA

3.1 RCO to evaluate controller's performance

This section illustrates the RCO, which plays a crucial role in adjusting the tuning scheme of the VCO-based model-free controller.

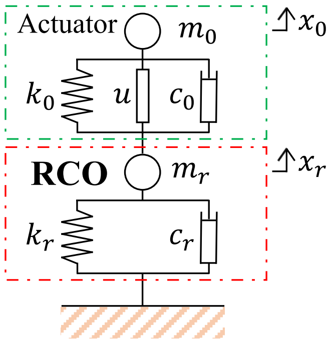

Fig. 4 RCO used for controller tuning.

Despite significant structural variations in controlled objects, the VCO-controller has demonstrated impressive robustness,[25,26] indicating that it remains effective across different controlled structures.

Consequently, this work utilizes the RCO-based model-free tuning method, capitalizing on its robustness. This auto-tuning specifies the proper controller's design variables through offline control simulations, which evaluate the RCO,[28,29] instead of the real controlled structure. In other words, the RCO represents an SDOF system defined on behalf of arbitrary controlled objects. The RCO, as shown in Fig. 4, is a designer-specified SDOF configuration with the mass, stiffness, and damping denoted as m_r, k_r, and c_r, respectively. Design policies for those parameters are presented as:

1) The RCO's scale needs to be greater than the actuator used to dampen vibrations. In other words, we should set m_r and k_r as $m_0 \ll m_r$ and $k_0 \ll k_r$, respectively. This requirement is necessary because the addition of a proof-mass actuator should not significantly change the characteristics of the actual plant when it is attached to a controlled object structure.
2) Let f_r be the natural frequency of the RCO. It is required to set m_r, k_r, and c_r so that $\Omega_2^{cont} > f_r > \Omega_1^{cont} \geq \sqrt{k_0/m_0}$ holds in the predetermined CFB. This is because a proof-mass actuator is applicable in the frequency band above $\sqrt{k_0/m_0}$. In addition, according to the guideline of the VCO-based model-free controller design,[25] f_r must present within $f \in (\Omega_1^{cont}, \Omega_2^{cont})$.

Although adjusting the controller based on the RCO does not require mathematical modeling of the real system, it is important to note that the optimized controller can also mitigate vibrations in other controlled objects within the CFB.[28,29] This is owing to the high robustness of the VCO-controller and the key condition $x_v \approx x_1$. The resilience of the VCO-based design approach arises from the fact that the resultant controller does not rely on the specific details (such as mathematical models and parameters) of the actual controlled systems.

3.2 Loss function

In iterative simulations designed to optimize the controller, a loss function (i.e., fitness measure) is utilized to evaluate the damping performance of VCO-based model-free controller for the RCO. The goal of the tuning process is to adjust the VCO-controller to minimize the loss function value. Let $\theta \in \mathbb{R}^p$ be the design variable of the VCO-controller. The loss function used in this study is given by[28]:

$$L(\theta) = \left\{W_y \times \left(\sum_{n=1}^{N} {y_n}^2\right) + W_u \times \left(\sum_{n=1}^{N} {u_n}^2\right)\right\} / N \tag{11}$$

where y_n denotes the controlled variable at the n-th sampling point, u_n represents the control effort at the n-th sampling point, N is the total number of sampling points, and $W_y = 1.0$ and $W_u = 30$ are the weights assigned to y_n and u_n, respectively. The variables y_n and u_n are derived from the vibration control simulation of the plant depicted in Fig. 4, using the VCO-controller parameterized by θ.

3.3 Tuning algorithm based on CGA[30,31,32]

This research adjusts the VCO-controller to minimize $L(\theta)$. Several studies have examined the minimization of the loss function (11) through the simultaneous perturbation stochastic approximation.[28,29] In contrast, the optimization problem is solved via the CGA owing to its good global search ability in this study, since CGA is designed as a population-based algorithm.[30,31,32]

Fig. 5 illustrates the tuning algorithm for a VCO-based model-free controller, where $C_{stop} \in \mathbb{N}$ represents the maximum number of iterations. At the k-th iteration, the j-th candidate solution is denoted as $\theta_k^{(j)} = \left[\theta_{k,1}^{(j)} \quad \theta_{k,2}^{(j)} \quad \cdots \quad \theta_{k,p}^{(j)}\right]^T \in \mathbb{R}^p$. The set of candidate solutions at the k-th iteration is $\wp_k = \left\{\theta_k^{(1)} \quad \theta_k^{(2)} \quad \cdots \quad \theta_k^{(Np)}\right\}$, where $N_p \in \mathbb{N}$ indicates the population size. The search range is constrained by the lower and upper bounds, denoted as lb and ub, respectively. The fitness function $F\left(\theta_k^{(j)}\right)$, defined as $-L(\theta_k^{(j)})$, is derived from the closed-loop simulation involving the VCO-controller with $\theta_k^{(j)}$ and the RCO. The CGA algorithm in Fig. 5 seeks the design variables maximizing the fitness, or equivalently, minimizing the loss function value. Each operation of CGA in Fig. 5 is as follows[30,31,32]:

(*Initial population*) The initial population $\wp_1$ is created randomly within the defined search range.

(*Parent selection and crossover*) In the k-th iteration, the candidate $\theta_k^{(j)}$ is selected as the parent $\varphi_k^{(j)}$ with probability of $\tilde{F}\left(\theta_k^{(j)}\right) / \left\{\sum_{j=1}^{Np} \tilde{F}\left(\theta_k^{(j)}\right)\right\}$, where $\tilde{F}\left(\theta_k^{(j)}\right) := F\left(\theta_k^{(j)}\right) + \left|\min_j F\left(\theta_k^{(j)}\right)\right|$. For a given pair of parents $\left\{\varphi_k^{(j)} \quad \varphi_k^{(j+1)}\right\}$, the crossover operation produces the offspring pair $\left\{\psi_k^{(j)} \quad \psi_k^{(j+1)}\right\}$ using the formulas $\psi_k^{(j)} = max\left(min\left(\tilde{\psi}_k^{(j)} \quad ub\right) \quad lb\right)$ and $\psi_k^{(j+1)} = max\left(min\left(\tilde{\psi}_k^{(j+1)} \quad ub\right) \quad lb\right)$, where max and min are the element-wise operation. Here, $\tilde{\psi}_k^{(j)} := r_j \cdot \varphi_k^{(j)} + (1 - r_j) \cdot \varphi_k^{(j+1)}$ and $\tilde{\psi}_k^{(j+1)} := (1 - r_j) \cdot \varphi_k^{(j)} + r_j \cdot \varphi_k^{(j+1)}$, with r_j being a random number uniformly distributed between 0 and 1. Finally, $\psi_k^{(j)}$ and $\psi_k^{(j+1)}$ are replaced by $\varphi_k^{(j)}$ and $\varphi_k^{(j+1)}$ with probability of $1 - P_c$, respectively.

(*Mutation*) Let $\varphi_{k,i}^{(j)}$ be the i-th component of $\varphi_k^{(j)}$. Then, $\varphi_{k,i}^{(j)}$ is replaced by $lb_i + rr(ub_i - lb_i)$ with probability of P_m, where $rr \in [0 \quad 1]$ is the uniformly distributed random number. In this expression, lb_i and ub_i represent the lower and upper limits for the i-th component of the design variable, respectively.

(*Next population*) The next population $\wp_{k+1}$ is composed of the N_e superior candidates in $\wp_k$ and $(N_p - N_e)$ candidates randomly chosen from $\left\{\varphi_k^{(1)} \quad \varphi_k^{(2)} \quad \cdots \quad \varphi_k^{(Np)}\right\}$.

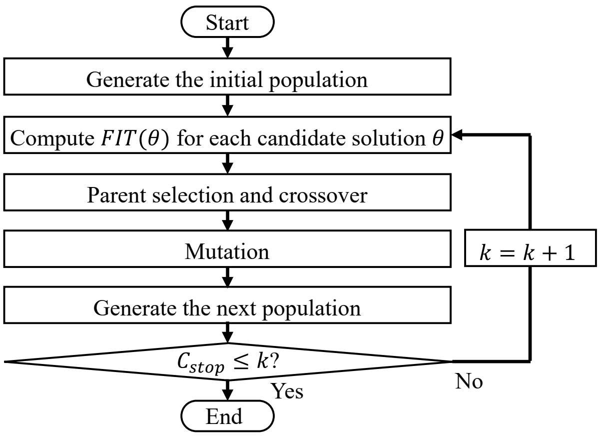

Fig. 5 Tuning algorithm based on CGA.

Table 2 indicates the settings for the CGA employed in this research. A 1–10000 Hz linear sweep sinusoidal signal is employed to excite the RCO in the iterative tuning simulations.

The purpose of the CGA algorithm is to autonomously identify the best values for the design variables. It is important to note that this method does not require the mechanical plant or the specific models of the controlled models. This is because the CGA only relies on the loss function values obtained from simulations with the RCO, rather than actual object models.

Table 2 Tuning conditions for CGA in this study.

Properties	Value
ub	$10^7 \times [1 \quad 1 \quad 1 \quad 1 \quad 1]^T$
lb	$[0 \quad 0 \quad 0 \quad 0 \quad 0]^T$
N_p	50
N_e	3
P_c	0.95
P_m	0.2
C_{stop}	4000
Disturbance to RCO	Linear sine sweep: 1–10000 Hz

4. APPLICATION OF PROPOSED TUNING TECHNIQUE

4.1 VCO-based model-free LQR

This paper employs the new tuning method for designing model-free LQR using VCO. In the context of the 2DOF system described by Eq. (12), which involves only the actuator and VCO, Eq. (13) specifies the performance index

$$\dot{x}_{mf} = A_{mf}x_{mf} + B_{mf1}w + B_{mf2}u \tag{12}$$

$$I(\theta) = \int_0^\infty \{x_{mf}{}^T Q(\theta) x_{mf} + u^T R(\theta) u\} dt. \tag{13}$$

Here, $I(\theta)$ represents the quadratic performance index for the VCO-based LQR design. The positive-definite matrix $Q(\theta) \in \mathbb{R}^{4\times4}$ and the positive scaler $R(\theta)$ are tuning parameters parametrized by the design variable θ (θ is determined by the algorithm shown in Fig. 5).

After VCO is properly designed, the model-free controller design simply follows a process of the standard LQR design.[33,34] It is widely acknowledged that, based on conventional LQR theory,[33,34] the control input designed to minimize $I(\theta)$ is specified in Eq. (14).

$$u = K_\theta x_{mf} = -R(\theta)^{-1} B_{mf2}{}^T P_\theta x_{mf} \tag{14}$$

where $P_\theta \in \mathbb{R}^{4\times4}$ represents the positive-definite solution to the algebraic Riccati equation given in Eq. (15):

$$A_{mf}{}^T P_\theta + P_\theta A_{mf} - P_\theta B_{mf2} R(\theta)^{-1} B_{mf2}{}^T P_\theta + Q(\theta) = 0. \tag{15}$$

In Eq. (14), the value of x_{mf} is obtained using the Kalman filter configured for Eq (6). To develop the LQR controller, the Control System Toolbox and Robust Control Toolbox in MATLAB are employed.

This paper automatically specifies θ for $Q(\theta)$ and $R(\theta)$ by the RCO-CGA-based tuning scheme described in the previous section. The tuning parameters, $Q(\theta)$ and $R(\theta)$, are adjusted by the proposed method. Using the notation in Section 3.3, the tuning parameters are parametrized by $\theta_k^{(j)}$ as

$$Q\left(\theta_k^{(j)}\right) = diag\left\{\left|\theta_{k,1}^{(j)}\right| \quad \left|\theta_{k,2}^{(j)}\right| \quad \left|\theta_{k,3}^{(j)}\right| \quad \left|\theta_{k,4}^{(j)}\right|\right\} Q_0 \tag{16}$$

$$R_k = \left|\theta_{k,5}^{(j)}\right| R_0. \tag{17}$$

The initial guesses of $Q(\theta)$ and $R(\theta)$ are indicated as Q_0 and R_0, respectively, and set as $Q_0 = diag\{1 \quad 1 \quad 1 \quad 1\}$ and $R_0 = 1$.

4.2 Tuning result

The tuning results obtained by the CGA are listed in Table 3 (θ_{Cstop}^* represents the optimal solution found by the proposed approach). Moreover, the iteration history of the loss function value is depicted in Fig. 6.

Table 3 Tuning result of the model-free LQR.

Properties	Value
$\theta_{Cstop,1}^*$	9.5269×10^6
$\theta_{Cstop,2}^*$	6.1312×10^3
$\theta_{Cstop,3}^*$	9.9257×10^6
$\theta_{Cstop,4}^*$	1.8509×10^6
$\theta_{Cstop,5}^*$	545.1332
J_1	0.901734
J_{Cstop}	0.442617

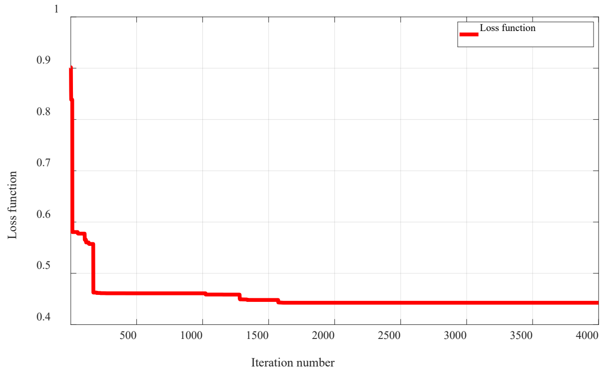

Fig. 6 History of the loss function.

Table 3 and Fig. 6 demonstrate that the iterative approach effectively reduces the value of the loss function. It is also observed from the comparison between J_1 and J_{Cstop} in Table 3 that the iterative optimization was successfully conducted.

To evaluate the performance of the tuned controller, the control simulation results for the RCO are shown in Fig. 7, where a 1–1000 Hz linear sweep sinusoidal signal was used as the disturbance.

(a)

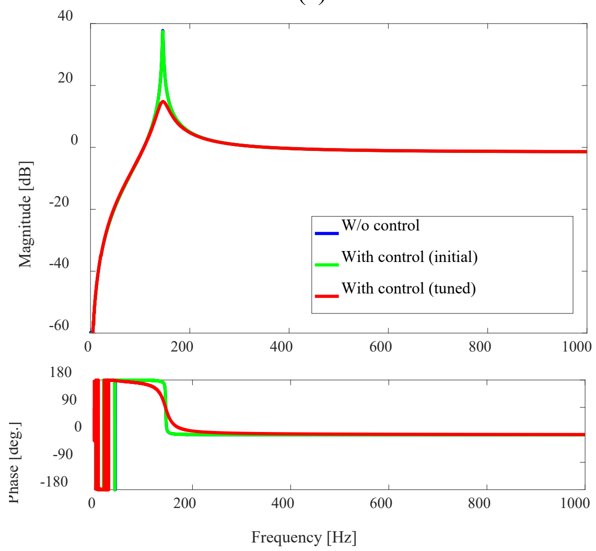

(b)

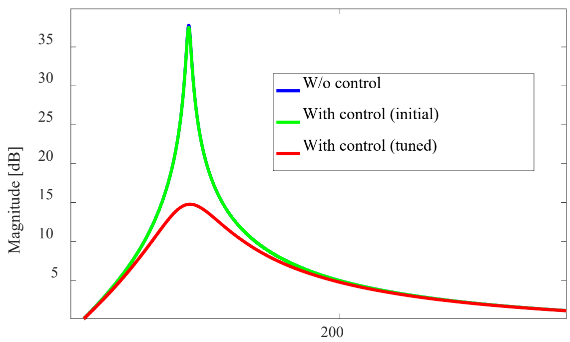

Fig. 7 Control result for RCO with a linear sweep sine signal (1–1000 Hz): (a) frequency response of the acceleration and (b) detailed view of the magnitude.

The responses indicated by the blue, green, and red lines represent the open loop, the initial untuned controller, and the controller tuned using the proposed method, respectively. As illustrated in Fig. 7, the tuned controller effectively mitigates the resonance peak, demonstrating its damping effect.

5. CONTROL SIMULATION

5.1 Verification settings

This paper applies the tuned controller to a more complex system other than the RCO to validate the vibration damping performance.

(a)

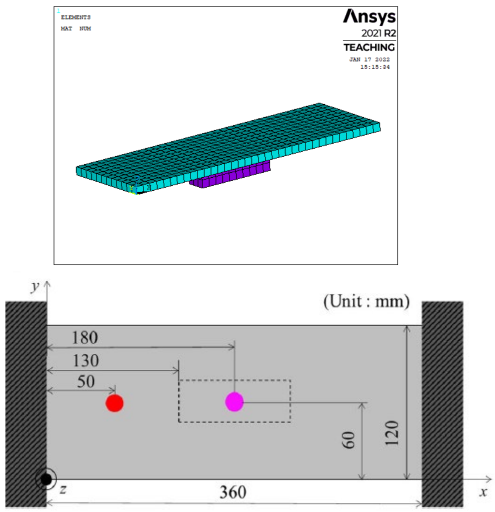

(b)

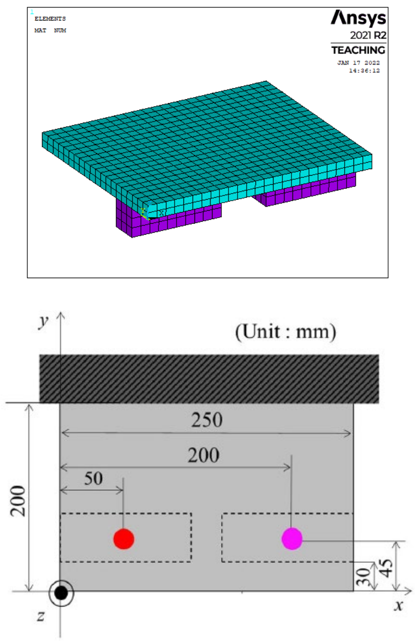

(c)

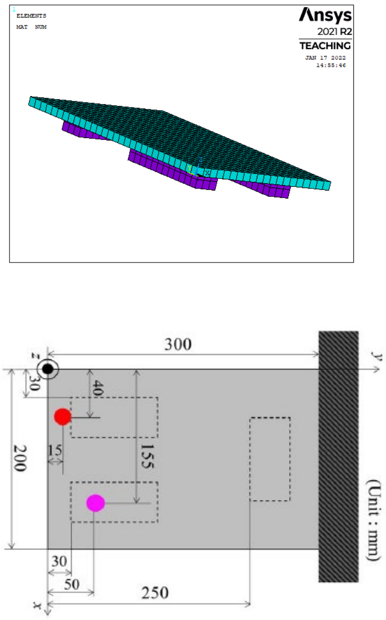

Fig. 8 FEM models and schematic representations of controlled structures[35]: (a) plate supported at both ends (Controlled object 1), (b) cantilever A (Controlled object 2), and (c) cantilever B (Controlled object 3).

As illustrated in Fig. 8, this study employs a plate supported at both ends and two types of cantilever plates as controlled objects, as detailed in our earlier research.[35] The structures depicted in Figs. 8(a)-(c) are designated as *Controlled objects 1, 2, and 3*, respectively. The control simulation incorporates the finite element method (FEM) models created by ANSYS. Refer the literature[35] for more detailed information on the FEM.

The disturbance used to shake the controlled structures is a linear sinusoidal signal with a frequency sweep ranging from 1 to 3000 Hz. As shown in Figs. 8(a)-(c), the acceleration response along the z-axis is measured at a location on the opposite plane from the actuator, and this is recorded as the observed output. Figure 8 highlights the locations of the control input and disturbance, marked by magenta and red points, respectively.[35]

Note that the specifications of the above FEM models do not affect the controller design. This is because the proposed vibration control method is model-free, meaning that it does not rely on any explicit knowledge of the system model, including FE mesh properties

5.2 Simulation result and discussion

The control simulation results of Controlled objects 1, 2, and 3 obtained by the tuned LQR are shown in Figs. 9-11, respectively. In simulation, a comparative evaluation is also involved with a manually tuned LQR,[27,28] which requires trial-and-error adjustments for obtaining sufficient vibration reduction.

(a)

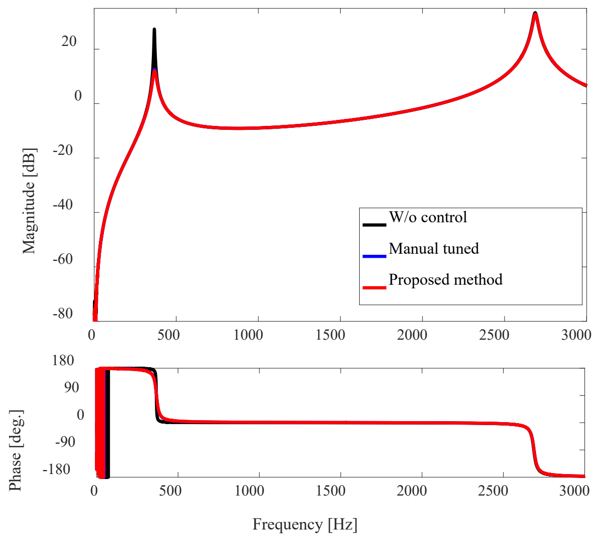

(b)

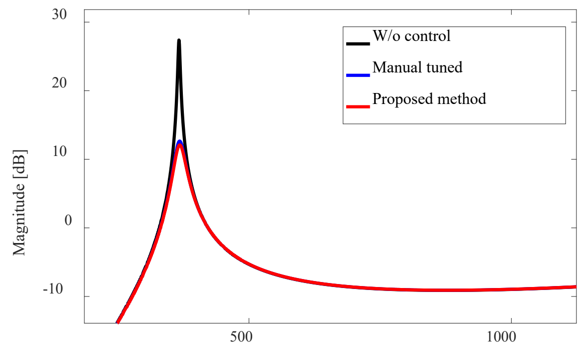

Fig. 9 Results for a plate supported at both ends (Controlled object 1) subjected to a linear sweep sine signal (1-3000 Hz): (a) frequency response of the acceleration output and (b) detailed view of the resonance peak in the low-frequency range.

(a)

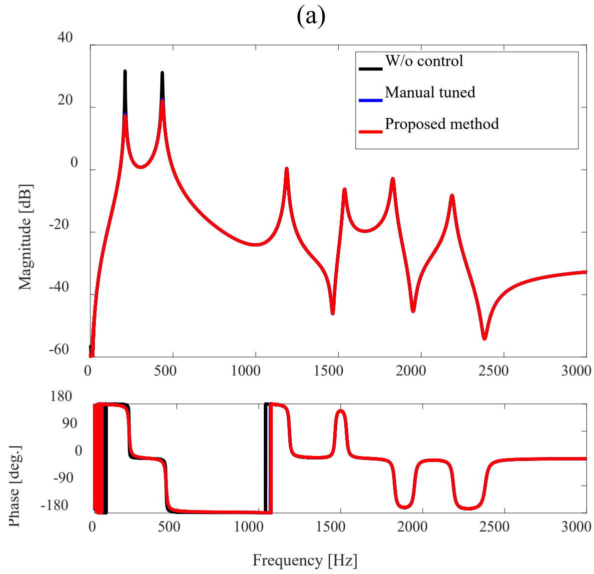

(b)

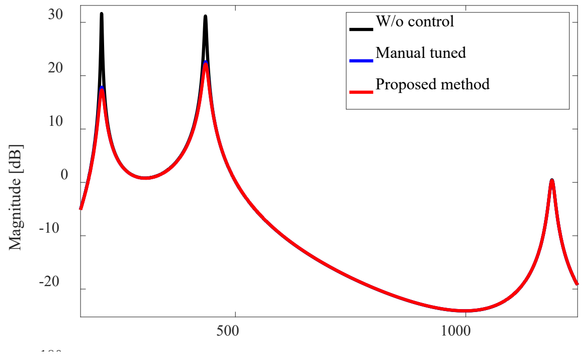

Fig. 10 Control result of a cantilever plate A (Controlled object 2) with linear sweep sine signal (1-3000 Hz): (a) frequency response of acceleration output and (b) detailed view of resonance peaks within a low-frequency range.

(a)

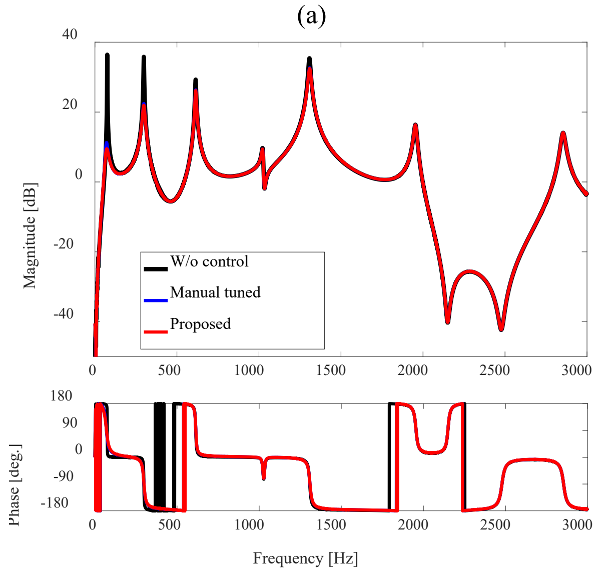

(b)

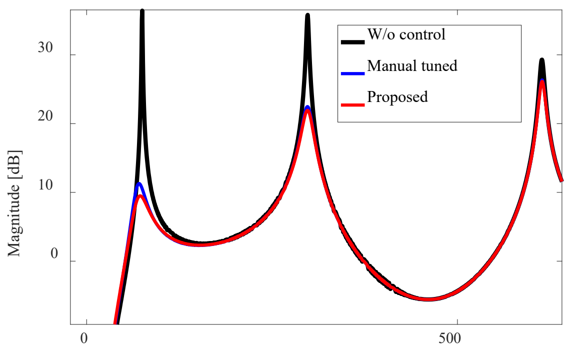

Fig. 11 Control result of a cantilever plate B (Controlled object 3) with linear sweep sine signal (1-3000 Hz): (a) frequency response of acceleration output and (b) a magnified depiction of the resonance peaks within a low-frequency range.

Table 4. Main peak suppression performance for a both-ends-supported plate (Controlled object 1).

Controller	Reduction amount [dB]
	366.6 Hz
Trial-and-error tuned LQR (i.e., manual tuned)	14.80
Auto-optimized LQR (i.e., proposed method)	15.38

Table 5. Main peak suppression performance for a cantilever plate A (Controlled object 2).

Controller	Reduction amount [dB]	
	209.5 Hz peak	435 Hz peak
Trial-and-error tuned LQR (i.e., manual tuned)	13.83	8.57
Auto-optimized LQR (i.e., proposed method)	14.38	9.03

Table 6. Main peak suppression performance for a cantilever plate B (Controlled object 3).

Controller	Reduction amount [dB]	
	75 Hz peak	298.1 Hz peak
Trial-and-error tuned LQR (i.e., manual tuned)	25.92	13.33
Auto-optimized LQR (i.e., proposed method)	27.13	13.88

According to the frequency responses of the controlled structures (Figs. 9-11), we can clearly evaluate the vibration attenuation performances achieved by the automatically tuned model-free LQR. These results indicate the successful tuning design by the CGA and RCO.

In contrast to the vibration reduction effects owing to the manual tuned LQR, the proposed tuning scheme provides the good attenuation performance at almost the same level, as indicated from comparison of the red and blue lines. Tables 4-6 quantitatively summarize the vibration reduction effects at the main resonance peaks in Figs. 9-11, respectively. Few differences exist in the damping performance between the two controllers, according to these quantitative comparisons of the results of the manually tuned LQR and the auto-tuned LQR. The remarkable implication from the above comparison is that the proposed approach significantly reduces a controller design effort through a simpler manner (i.e., automated tuning process), compared to the manual tuning design. The reason is that the suggested method avoids the need for subjective trial-and-error adjustments for $Q\left(\theta_k^{(j)}\right)$ and R_k, achieving performance similar to that of the manually tuned LQR. As a result, this automatic tuning approach delivers a model-free damping system more efficiently without compromising vibration attenuation capabilities.

Despite the differences in dimensions and boundary conditions among the three structures shown in Figs. 8(a), (b), and (c), the proposed method demonstrates vibration suppression effects in the low-frequency band for all structures, as shown in Tables 4-6. This is because the VCO-based model-free control does not rely on information about the vibration modes or natural frequencies of the structures, thereby exhibiting robustness against their variations. In fact, the condition in Eq. (4) indicates that, in principle, all vibrations can be suppressed as long as the vibrations occurring at the damping point are within the controlled bandwidth and the crucial condition $x_v \approx x_1$ is satisfied. Theoretically, this condition is independent of the shape of the vibration modes of the controlled structures. However, in practical applications, there are limitations on vibration suppression performance. This is because if the actuator is placed at a node of the vibration mode of the controlled structure, it cannot transfer the excitation needed to apply the control input. This limitation can be inferred from the fact that the vibration suppression effect in the high-frequency band above 1000 Hz is almost absent in the control results shown in Fig. 10.

The successful setup of the VCO and RCO plays a key role in the model-free active damping. The validity of their setup in this research was supported by the numerical validation results in which vibrations occurring in the various structures are commonly attenuated despite the fact that offline iterative simulations during the tuning process employ only the RCO. Moreover, a notable aspect is that no models or parameters of the structures shown in Fig. 8 (i.e., Controlled objects 1, 2, and 3) are used in the derivation process of the VCO-based model-free controller. This detailed-structure-independent nature of the VCO-based design makes it possible to apply the resultant controller to various structures other than VCO or RCO because the robustness is enforced, as pointed out by the previous literatures.[25,27] In fact, even though there are characteristic changes among the different structures (i.e., Controlled objects 1, 2, and 3), the proposed control system exhibits the sufficient damping performances without instability, indicating its independency of specific phenomena of the controlled structures.

Previous studies employ gradient-based optimization techniques, such as simultaneous perturbation stochastic approximation, to adjust an active damping controller.[28,29] In contrast to the prior works, one of the advantages of employing CGA is its independence from careful selection of initial values. This is owing to the global search capability based on the more random algorithm. In the previous literature,[28] it was necessary to carefully select some appropriate initial values for the optimization algorithm to be performed successfully. It is because a gradient-based optimization algorithm tends to strongly depend on initial design variables $\theta_k^{(j)}$. In this work, the introduction of CGA into the tuning algorithm contributes to alleviating this issue.

In the application scenario, the actuator is attached directly at the damping point at which the occurred vibrations should be suppressed and provides a control force perpendicular to the structure surface. The mechanical principle is also applicable to serial-link industrial robots employed in precision robotic machining process[36] and inertial-mass actuators for civil structures.[37] In the robotic milling,[36] the low-stiffness-induced chatter can be attenuated by directly installing an inertial voice coil actuator near the source of excitation on the robot. For civil structures, the proposed configuration may be applied to actively damp vibrations due to human-induced excitations in floor systems[37] or lightweight footbridges by attaching an inertial-mass actuator on the surface of the floor.

Compared to applications of machine learning such as Deep Neural Networks (DNN)-based approaches,[38] which may be extended to controller optimization, the key advantage of our proposed method is that it does not require the collection of large datasets from the controlled structures, making it easier to implement. VCO-based model-free design does not require modeling of the controlled structures or extensive trial-and-error control experiments; therefore, it can be more quickly implemented. Additionally, unlike DNN-based approaches, overfitting is not an issue in our approach because the proposed design process is independent of datasets from real controlled structures.

On the other hand, our method has some weaknesses. The actuator needs to be a proof-mass actuator, modeled as a single-degree-of-freedom system. Additionally, our study does not fully analyze how much variation in the controlled structure can be tolerated while maintaining robustness. Addressing these limitations remains a challenge for future research.

6. CONCLUSION

In this paper, a novel model-free tuning method for an active oscillation controller is introduced, utilizing a CGA-based approach. The design of this model-free damping controller incorporates the concept of VCO and RCO to assess the damping level quantitatively. The CGA is used to automatically determine the optimal controller parameters by minimizing the loss function value. The efficacy of the resulting vibration controller is validated through numerical examples across various mechanical systems, including unknown cantilever plates, and is compared to a controller tuned through trial and error. The new outcome is that the proposed model-free auto design scheme can ensure high damping performances and robustness for different structures (a plate supported at both ends and two cantilever plates) with characteristic variations and changed boundary conditions. This robustness can be attributed to the detailed-specification-independent nature provided by the controller design process that does not rely on any specific plant modeling. As the representative results, the resonance peaks of Controlled object 1 (both-ends-supported plate), Controlled object 2 (cantilever plate A), and Controlled object 3 (cantilever plate B) in the low-frequency band were attenuated by 15.38 dB, 14.38 dB and 27.13 dB, respectively. These damping levels have almost the same levels as those by a manual tuned controller; however, the proposed method significantly reduced the development costs.
The primary focus of this study is on the fundamental investigation of the proposed approach through comprehensive simulations. Experimental validation is an important future research direction.

Acknowledgments
This research was funded by the Japan Society for the Promotion of Science through Grants-in-Aid for Scientific Research Programs (Grant no. 23K13273).

Declaration of conflicting interests
The author(s) declared no potential conflicts of interest with respect to the research, authorship, and/or publication of this article.

Funding
The author(s) disclosed receipt of the following financial support for the research, authorship, and/or publication of this

article: This work was supported by the Japan Society for the Promotion of Science under Grants-in-Aid for Scientific Research Programs (Grant no. 23K13273).

REFERENCES

1. Tang J, Cao D, Yu T. Decentralized vibration control of a voice coil motor-based Stewart parallel mechanism: Simulation and experiments. *Proc Inst Mech Eng Part C J Mech Eng Sci* 2019; 233: 132–145.
2. Eser S, Çetin ST. Optimum control of a flexible single link manipulator with Artificial Bee Colony Algorithm. *Proc Inst Mech Eng Part C J Mech Eng Sci* 2022; 236: 3731–3742.
3. Errico F, Petrone G, Rosa S De, et al. On the concept of embedded resonators for passive vibration control of tyres. *Proc Inst Mech Eng Part C J Mech Eng Sci* 2021; 235: 2587–2593.
4. Nie J, Yang Y, Jiang T, et al. Passive Skyhook Suspension Reduction for Improvement of Ride Comfort in an Off-Road Vehicle. *IEEE Access* 2019; 7: 150710–150719.
5. Yonezawa H, Yonezawa A, Kajiwara I. Novel Powertrain Vibration Controller With Six Rules-Based Fuzzy Inference for Time-Fluctuated Control Period. *IEEE Access* 2024; 12: 11972–11986.
6. Yonezawa H, Yonezawa A, Kajiwara I. Efficient Tuning Scheme of Mode-Switching-Based Powertrain Oscillation Controller Considering Nonlinear Backlash. *IEEE Access* 2023; 11: 93935–93947.
7. Li L, Zhang Q, Zhang T, et al. Vibration suppression of ball-screw drive system based on flexible dynamics model. *Eng Appl Artif Intell* 2023; 117: 105506.
8. Jinyu Z, Song H, Longyu J, et al. Active Vibration Control Strategy for Online Application in a Range Extender. *IEEE Access* 2023; 11: 26686–26702.
9. Yonezawa H, Kajiwara I, Nishidome C, et al. Active vibration control of automobile drivetrain with backlash considering time-varying long control period. *Proc Inst Mech Eng Part D J Automob Eng* 2021; 235: 773–783.
10. Yonezawa H, Yonezawa A, Hatano T, et al. Experimental verification of active damping of powertrain vibrations with simple fuzzy logic compensation for time-varying control period. *Proc Inst Mech Eng Part D J Automob Eng* 2023; 095440702311781.
11. Jang JSR, Sun CT. Neuro-Fuzzy Modeling and Control. *Proc IEEE* 1995; 83: 378–406.
12. Madan A. Vibration control of building structures using self-organizing and self-learning neural networks. *J Sound Vib* 2005; 287: 759–784.
13. Zhao S, Gao Z. An Active Disturbance Rejection Based Approach to Vibration Suppression in Two-Inertia Systems. *Asian J Control* 2013; 15: 350–362.
14. Ju Y, Fang C, Zhou H, et al. Transverse vibration analysis and active disturbance rejection decoupling control of rain erosion whirling arm. *Proc Inst Mech Eng Part C J Mech Eng Sci*. Epub ahead of print 17 June 2024. DOI: 10.1177/09544062241255574.
15. Yahagi S, Kajiwara I, Shimozawa T. Slip control during inertia phase of clutch-to-clutch shift using model-free self-tuning proportional-integral-derivative control. *Proc Inst Mech Eng Part D J Automob Eng* 2020; 234: 2279–2290.
16. Ramírez-Neria M, Morales-Valdez J, Yu W. Active vibration control of building structure using active disturbance rejection control. *J Vib Control* 2022; 28: 2171–2186.
17. Yan X, Xu Z-D, Shi Q-X. Fuzzy neural network control algorithm for asymmetric building structure with active tuned mass damper. *J Vib Control* 2020; 26: 2037–2049.
18. Konoiko A, Kadhem A, Saiful I, et al. Deep learning framework for controlling an active suspension system. *J Vib Control* 2019; 25: 2316–2329.
19. Saeed MU, Sun Z, Elias S. Research developments in adaptive intelligent vibration control of smart civil structures. *J Low Freq Noise, Vib Act Control* 2022; 41: 292–329.
20. Ahmed S, Wang H, Tian Y. Model-free control using time delay estimation and fractional-order nonsingular fast terminal sliding mode for uncertain lower-limb exoskeleton. *J Vib Control* 2018; 24: 5273–5290.
21. Li S, Zhu C, Mao Q, et al. Active disturbance rejection vibration control for an all-clamped piezoelectric plate with delay. *Control Eng Pract* 2021; 108: 104719.
22. Wang HP, Mustafa GIY, Tian Y. Model-free fractional-order sliding mode control for an active vehicle suspension system. *Adv Eng Softw* 2018; 115: 452–461.
23. Zhang J, Long F, Lin J, et al. Particle swarm optimized fuzzy proportional-integral-derivative controller-based transverse leaf spring active suspension for vibration control. *J Low Freq Noise, Vib Act Control* 2024; 43: 979–996.
24. Hadi MS, Darus IZM, Tokhi MO, et al. Active vibration control of a horizontal flexible plate structure using intelligent proportional–integral–derivative controller tuned by fuzzy logic and artificial bee colony algorithm. *J Low Freq Noise, Vib Act Control* 2020; 39: 1159–1171.
25. Yonezawa H, Kajiwara I, Yonezawa A. Experimental verification of model-free active vibration control approach using virtually controlled object. *JVC/Journal Vib Control* 2020; 26: 1656–1667.

26. Yonezawa A, Yonezawa H, Kajiwara I. Experimental study of model-free vibration control based on a virtual controlled object considering parameter uncertainty of actuator. *Proc Inst Mech Eng Part C J Mech Eng Sci* 2023; 237: 2665–2674.
27. Yonezawa A, Yonezawa H, Kajiwara I. Vibration control for various structures with time-varying properties via model-free adaptive controller based on virtual controlled object and SPSA. *Mech Syst Signal Process* 2022; 170: 108801.
28. Yonezawa A, Yonezawa H, Kajiwara I. Parameter tuning technique for a model-free vibration control system based on a virtual controlled object. *Mech Syst Signal Process* 2022; 165: 108313.
29. Yonezawa A, Yonezawa H, Kajiwara I. Efficient parameter tuning to enhance practicability of a model-free vibration controller based on a virtual controlled object. *Mech Syst Signal Process* 2023; 200: 110526.
30. Holland JH. Genetic Algorithms. *Sci Am* 1992; 267: 66–73.
31. Haupt RL, Haupt SE. *Practical genetic algorithms*. Wiley-Interscience, 2004.
32. Ignaciuk P, Wieczorek Ł. Continuous Genetic Algorithms in the Optimization of Logistic Networks: Applicability Assessment and Tuning. *Appl Sci* 2020; 10: 7851.
33. Kalman RE. On the general theory of control systems. *IFAC Proc Vol* 1960; 1: 491–502.
34. Åström KJ, Murray RM. *Feedback Systems: An Introduction for Scientists and Engineers, Princeton University Press, Princeton*. New Jersey, 2009.
35. Sato Y, Yonezawa H, Yonezawa A, et al. Stability Improvement of Model-Free Control Based on a Virtual Structure Against the Resonance of a Proof-Mass Actuator. *J Vib Eng Technol* 2022; 10: 1175–1188.
36. Zhang R, Wang Z, Keogh P. H-infinity optimised control of external inertial actuators for higher precision robotic machining. *Int J Comput Integr Manuf* 2022; 35: 129–144.
37. Pereira E, Díaz IM, Hudson EJ, et al. Optimal control-based methodology for active vibration control of pedestrian structures. *Eng Struct* 2014; 80: 153–162.
38. Samaniego E, Anitescu C, Goswami S, et al. An energy approach to the solution of partial differential equations in computational mechanics via machine learning: Concepts, implementation and applications. *Comput Methods Appl Mech Eng* 2020; 362: 112790.